Trans Indian Inst Met (2026) 79:37
https://doi.org/10.1007/s12666-026-03790-4

ORIGINAL ARTICLE

Numerical Analysis and Experimental Monitoring of Blast Furnace Blowpipe Surface Temperature Utilizing FBG Sensors

Y. Usha[1] · S. Tewary[1] · A. Ghosh[1] · C. Dutta[1] · Alok Kumar[3] · T. K. Das[1] · P. Biswas[2] · S. Bandyopadhyay[2] · R. S. Sundaram[3] · S. Balamurugan[3] · S. Palit Sagar[1]

Received: 24 September 2024 / Accepted: 12 January 2026 / Published online: 30 January 2026

Abstract Industrial metals, such as pig iron, are produced in blast furnaces within the steel industry. During the smelting process in a blast furnace, a hot blast of air, exceeding 1373 K, flows through the blowpipe. The refractory lining of the blowpipe is prone to erosion and thermal cracking due to hostile operating conditions. Any unnoticed erosion of a refractory liner at an inaccessible site may lead to blowpipe rupture. In the present investigation, numerical computations were performed using computational fluid dynamics (CFD) analysis to investigate the thermal profiles of similar abnormal or defective situations at varying distances from the blowpipe tip, thereby aiding in the appropriate positioning of sensors on the blowpipe surface. The numerically computed temperature profile of the blowpipe surface under an ideal case, without any abnormalities, was validated with the online plant data obtained from fiber Bragg grating (FBG) sensors embedded on the blowpipe surface. Thus, the simulated thermal profiles obtained through CFD analysis will be beneficial in ascertaining the anomalous condition of the blowpipe that occurs due to erosion.

Keywords Anomaly simulation · Blast furnace blowpipe · Fiber bragg grating sensor · Numerical modeling

✉ Y. Usha
usha.nml@csir.res.in

1 CSIR-National Metallurgical Laboratory, Jamshedpur, India

2 CSIR-Central Glass and Ceramic Research Institute, Kolkata, India

3 NDT & Sensors Research Group, R&D Tata Steel, Jamshedpur, India

1 Introduction

Smart maintenance and industrial real-time condition monitoring are essential for realizing Industry 4.0 [1]. In this context, computational fluid dynamics (CFD) analysis, in particular, conjugate heat transfer (CHT) studies, has been found to be quite helpful in evaluating the thermal and flow behavior of large and complex engineering structures in industrial plant environments [2] [3] [4]. The blowpipe is a critical component in a blast furnace, connecting to the tuyeres. The hot air flowing through the blowpipe at high temperature and pressure makes the blowpipe susceptible to erosion and subsequent rupture. This could result in any critical catastrophe, such as a blowpipe bursting and untimely process downtime. Online structural health monitoring of the blowpipe is crucial for ensuring the safety of the steel plant and preventing inconvenient downtime or hazardous conditions. Failure analysis of industrial structures exposed to elevated temperatures [5], specifically blowpipe structural damage involving the prediction of the microstructure in crack zones to locate the brittle fracture region, is reported in [6]. Investigations on blowpipe bulging in a blast furnace are reported in [7], which comprised a detailed visual examination along with physical and chemical characterization of the blowpipe material. The blowpipe bulging has been reported to be the consequence of localized heating of the refractory lining at elevated temperatures, at around 1200 °C. The prolonged exposure to high temperatures resulted in thermal instability, leading to the initiation of the blowpipe damage due to refractory lining cracking. Several researchers have reported material damage [8] and its associated microstructural changes at elevated temperatures [5]. Researchers have also performed CFD investigations to understand the flow and thermal stress behavior in the blast furnace blowpipe [9, 10]. However, CFD modeling has not yet been explored for blowpipe anomaly situations to generate the corresponding thermal profiles.

Thermal imaging is a widely used technique for monitoring the criticality of industrial structures. Infrared thermography is a well-known nondestructive evaluation method for generating the thermal profile of any structure. In our previous study, we identified a limitation of thermography for the blowpipe due to the inaccessibility of half of its surface [11]. Therefore, infrared thermography may not be suitable for real-time surface temperature monitoring of the blowpipe. As a preventive measure, thermocouples were installed for real-time monitoring, and a temperature above 480 ˚C was considered for blowpipe shutdown [12]. Since placing multiple thermocouples in such a large industrial structure during plant operation complicates the arrangement, both IR thermography and the existing thermocouple arrangements are unsuitable for real-time monitoring. FBG sensors are widely used in structural health monitoring applications because they can precisely measure localized strain and temperature, have high sensitivity, and are well-suited for operation in harsh environments [13]. Therefore, in the present investigation, the fiber Bragg grating (FBG) sensors with proper packaging are considered for real-time temperature monitoring and to validate the CFD-based numerical simulations.

2 Materials and Methods

2.1 Computational Domain in Numerical Analysis

Conjugate heat transfer (CHT) analysis was carried out to solve the coupled conduction–convection control volume. The CHT model, as shown in Fig. 1, was performed on the computational domain of the industrial blowpipe, which comprises an alumina refractory lining enclosed within a metallic sheath, and the respective fluid and solid domains are represented. The discretization of the 3D blowpipe involves a grid-independent study, wherein the optimal number of nodes obtained is 10,88,414 using the *Ansys* mesh solver. The numerical analysis was conducted on a workstation equipped with an *Intel*$^{(R)}$ *Xeon*$^{(R)}$ CPU featuring eight cores.

Figure 1 demonstrates the solid domain comprising the sheath and the refractory liner, along with the direction of hot-air fluid flow toward the tip of the blowpipe to the tuyere.

Both the ideal and anomalous conditions of the blowpipe were considered in the present work, as described in Fig. 2. In the ideal case, there is no blowpipe failure, and this case idealizes the refractory liner without any cracks/erosion. As shown in the cross-sectional view of the blowpipe in Fig. 2a and b, the hatched zone is the solid domain comprising steel sheath and alumina refractory, and the remaining unhatched zone is the fluid domain.

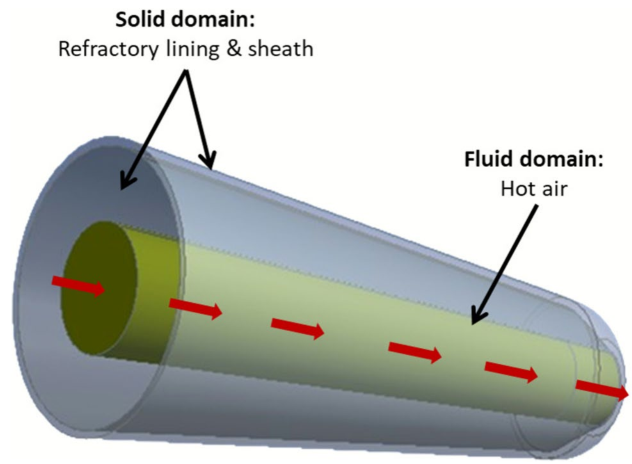

Fig. 1 3D Blowpipe conjugate heat transfer computational domain

Furthermore, anomaly cases were investigated to analyze the effect of anomalies or refractory erosion on the thermal distribution on the blowpipe surface, aiding in the positioning of the sensors for real-time monitoring. Herein, the refractory liner of the blowpipe considered was partially/fully eroded, wherein the computational domain was considered with the refractory lining in a deteriorated condition. An example of such refractory lining erosions, with partial or through erosion at two different locations, is shown in Fig. 2c and d.

2.2 Numerical Model Description

Based on the process parameters obtained from the plant, as mentioned in Table 1, the boundary conditions were applied to the computational domain with an incompressible hot-air velocity inlet and pressure outlet boundary conditions, along with no-slip, stationary, adiabatic walls, for numerically solving the steady-state Reynolds-averaged Navier–Stokes (RANS) equations using a pressure-based solver in *Ansys Fluent 19.0* [14]. The boundary conditions involved in the present conjugate heat transfer analysis are:

Hot-air velocity inlet at the entry, $u_{in} = 65m/s, T_{in} = 1473$ K

Pressure outlet at the blowpipe tip, $\boldsymbol{p_{out}} = \boldsymbol{p_{atm}} = 3.7\boldsymbol{bar}$

Remaining walls, $\vec{\boldsymbol{v}}_{\boldsymbol{fluid}} = \vec{\boldsymbol{v}}_{\boldsymbol{wall}} = 0$; $\boldsymbol{n}.(-\boldsymbol{k}\nabla\boldsymbol{T}) = 0$ (no-slip, stationary and adiabatic wall).

External ambient temperature, $\boldsymbol{T_a} = 350\mathbf{K}$

Herein, the Semi-Implicit Method for Pressure Linked Equations (SIMPLE) scheme was employed for pressure–velocity coupling, and the second-order upwind method was used for spatial discretization.

Table 2 lists the thermophysical properties of the fluid/solid domain and the materials involved.

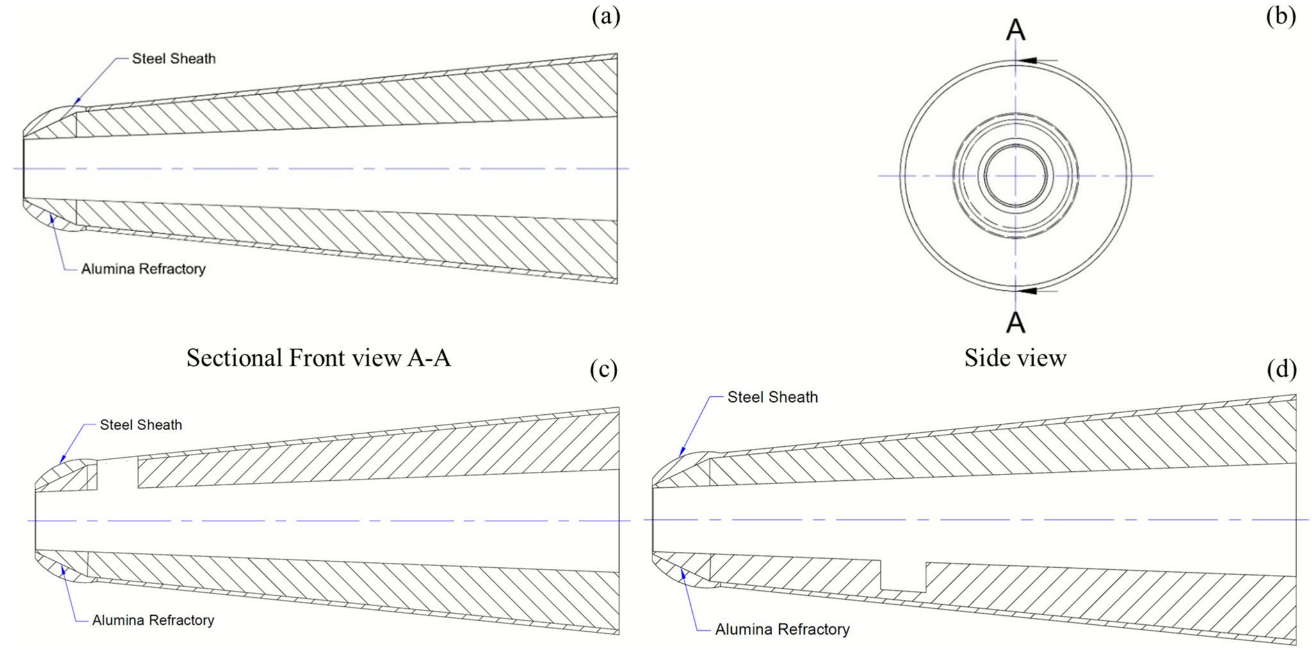

Fig. 2 Blowpipe: (**a**) & (**b**) Ideal case; (**c**) & (**d**) through and partially eroded at 150 and 500 mm from the blowpipe tip, respectively

Table 1 Process parameters used in the present analysis

Property	Value
Hot blast pressure	3.7 bar
Tuyere velocity	212 m/s
Hot-air inlet temperature	1473 K
External environment temperature	350 K

Governing equations with an assumption of constant property flow involved are:

$$\text{Continuity}: div(\vec{v}) = 0 \quad (1)$$

$$\text{Modeled RANS}: \rho\frac{D\vec{V}}{Dt} = -\nabla p + (\mu + \mu_t)(\nabla^2\vec{V}) \quad (2)$$

whereas turbulent viscosity is solved using the standard k-ε with the standard wall function.

$$\text{Heat equation in the fluid}: \rho_f C_f \frac{DT_f}{Dt} = \nabla.(k_f \nabla T_f) + \Phi^{\cdot} \quad (3)$$

wherein, Φ represents the viscous dissipation, and *f*-subscript represents the fluid material properties.

$$\text{Heat equation in the solid}: \rho_s C_s \frac{\partial T_s}{\partial t} = \nabla.(k_s \nabla T_s) \quad (4)$$

Herein, *s*-subscript represents the solid material properties.

Table 2 Thermophysical properties used in the present analysis

Domain	Material	Property	Value
Fluid	Hot air	Thermal conductivity	0.0242 W/m–K
		Density	1.225 kg/m^3
		Specific heat	1006.43 J/kg-K
		Viscosity	1.7894e-05 kg/m-s
Solid	Alumina refractory	Thermal conductivity	0.67 W/m–K
		Density	1000 kg/m^3
		Specific heat	1000 J/kg-K
	Steel ASTM 516 Gr 70 (Sheath)	Thermal conductivity	50 W/m–K
		Density	8030 kg/m^3
		Specific heat	502 J/kg-K

2.3 Anomaly Analysis Strategy

Numerical computations were performed for various anomaly situations, considering a solid computational domain with a fully eroded refractory liner of 10 mm diameter, as described in Sect. 2.1. Since the sensor can be practically placed starting from 100 mm near the blowpipe tip, simulations were conducted at every 100-mm interval from the blowpipe tip to investigate the thermal distribution. As reported in the literature, refractory liner failure was usually observed up to the center of the blowpipe due to localized overheating [7], so the simulation cases were considered up to the center of the blowpipe. This simulation helped in deciding the optimal sensor placement on the surface of the blowpipe (Table 3).

2.4 Experimental FBG Sensor Arrangement

The FBG sensors operate based on the Fresnel reflection principle, wherein when light travels between two media with different refractive indices, it will have both reflection and refraction at the interface [15]. In a Bragg grating, a periodic change in refractive index is generated within the optical fiber core, which reflects a small spectral component of the broadband light source [16]. The wavelength of light that is reflected, called the Bragg wavelength, is connected to the period of the grating, defined by:

$$\lambda_B = 2n_e\Lambda \quad (5)$$

where n_e is the effective refractive index, and Λ is the grating period in the core of the optical fiber. In optical fibers, gratings are inscribed to measure physical parameters, such as strain and temperature, by monitoring the Bragg wavelength shift during operation [17]. FBG sensors deployment for the structural health monitoring applications is reported in the literature [18, 19]. The advantage of FBG sensors over conventional thermocouples is that multiple FBGs can be written on a single optical fiber, making it more straightforward for dynamic monitoring [20, 21]. In this work, FBG sensors were embedded on the surface of the blowpipe for real-time temperature measurement at its various locations covering the entire blowpipe structure circumferentially. To validate the ideal case simulation results without any refractory liner erosion, temperature inputs were taken from the functional blowpipe in the plant. The FBG sensors array embedded depth on the blowpipe steel sheath was approximately 3 mm from the outer surface of the steel sheath. Four arrays, each having five FBG sensors, were used, and a total of 20 sensor data points were considered for measurement from the four arrays connected to four input channels of the *si-155* interrogator, manufactured by *Micron Optics*, located in the control room. The sensors were calibrated by measuring the wavelength shifts at different temperatures, viz. room temperature, 323, 348, 373 … 723 K inside a tubular furnace. Five sets of measurements were taken, and the average wavelength shift was recorded for the calibration coefficients of the FBG sensor.

3 Results and Discussion

The ideal blowpipe case was numerically analyzed, and the obtained temperature distribution was experimentally compared with the numerical results. The maximum temperature at the blowpipe tip gradually decreases in steps while moving away from the tip due to the variation in refractory lining thickness as shown in Fig. 3. The minimum and maximum refractory lining thickness is 5 mm at the blowpipe tip and 139 mm at the hot-air entry, respectively, as shown in Fig. 1. In this case, the peak temperature is expected to be located at the blowpipe tip, which is more susceptible to localized overheating, resulting in the deterioration of the blowpipe refractory liner.

The temperature distribution contour of anomaly cases with refractory liner erosion, as shown in Fig. 4, follows the maximum temperature at the eroded position due to a reduction in liner thickness in the confined region.

Based on the temperature distribution contour of the ideal case, it is evident that the maximum temperature is obtained at the blowpipe tip when compared to other positions, and in anomaly blowpipe situation, peak temperature is observed at the site of the refractory liner erosion. Therefore, FBG packaging is considered with a larger number of sensors arranged close to the blowpipe tip due to the likelihood of localized heating. Four arrays of FBG sensors were packed, with each array comprising five FBG sensors, resulting in a total of 20 sensor data points being measured. The two arrays are shown in Fig. 5, and the other two arrays were symmetrically embedded on the blowpipe surface for real-time temperature monitoring during plant operation.

FBG sensors with safety protection were utilized during the experiments to measure the actual temperature variations. Detected peaks in four FBG sensor arrays for temperature measurement, where shifts in peaks correspond to temperature change, are shown in Fig. 6.

Table 3 Anomaly situations at varied locations

Location of the through-thickness refractory lining erosion from the blowpipe tip (worst-case scenarios at different locations)	100 mm (near tip), 200 mm, 300 mm, 400 mm, 500 mm, 600 mm, and 700 mm (center)

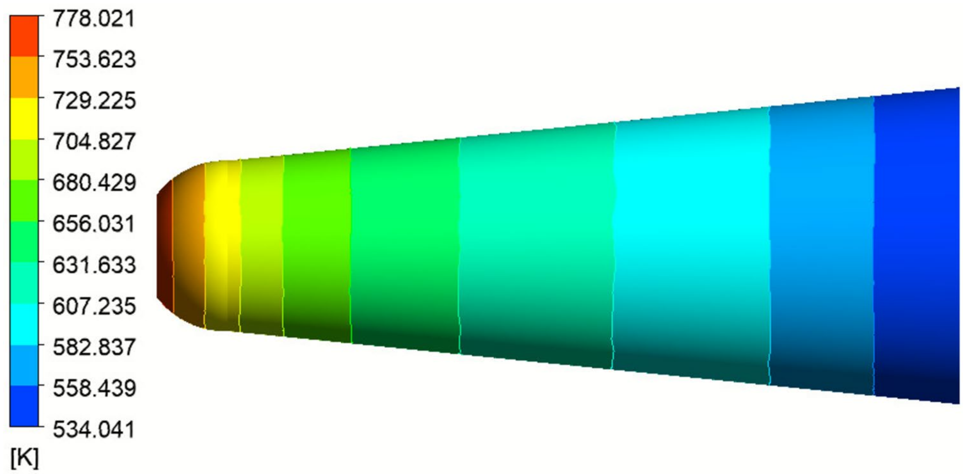

Fig. 3 Temperature distribution obtained from the simulation of an ideal blowpipe without an anomaly

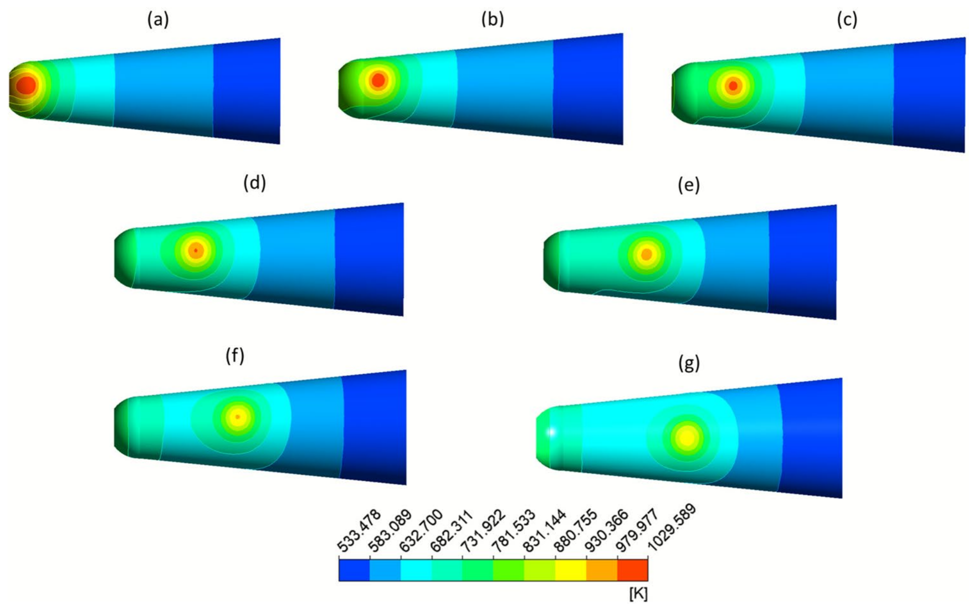

Fig. 4 Simulated temperature distribution for anomaly cases with refractory lining erosion at **a** 100, **b** 200, **c** 300, **d** 400, **e** 500, **f** 600, and **g** 700 mm from the blowpipe tip

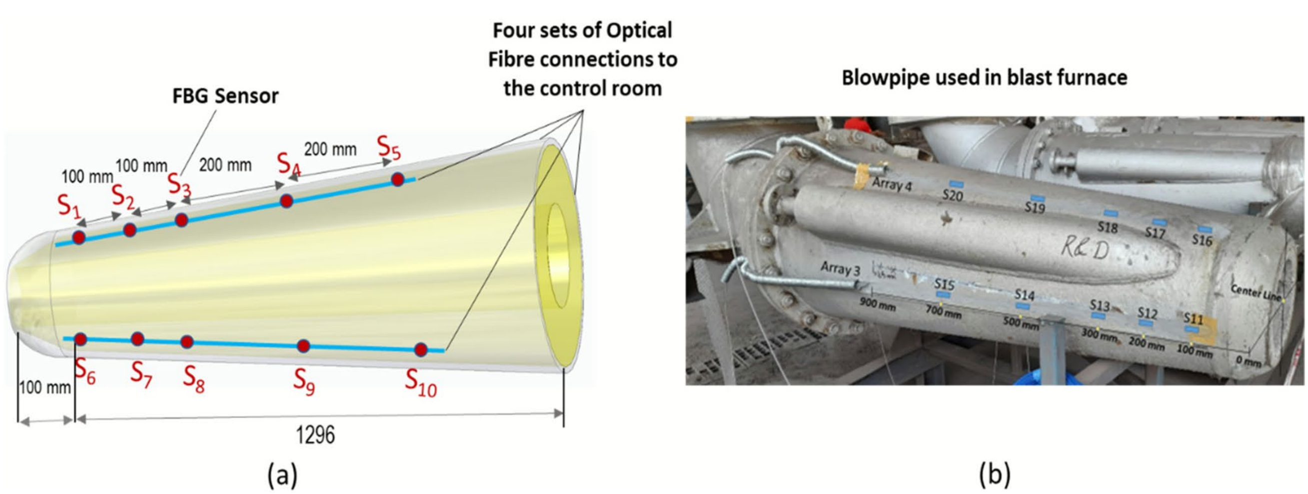

Fig. 5 **a** FBG sensor arrangement embedded on the blowpipe surface and **b** real-time FBG sensor embedded on the blowpipe surface

Figure 7 validates the simulation data against the experimentally obtained temperature distribution for the ideal blowpipe case without any refractory liner erosion. The temperature distribution obtained from the simulation results showed a similar trend to the real-time temperature information gathered from the sensors over the 7-day period of the average temperature measurement. However, minor variations in the temperature pattern were observed for Array 4,

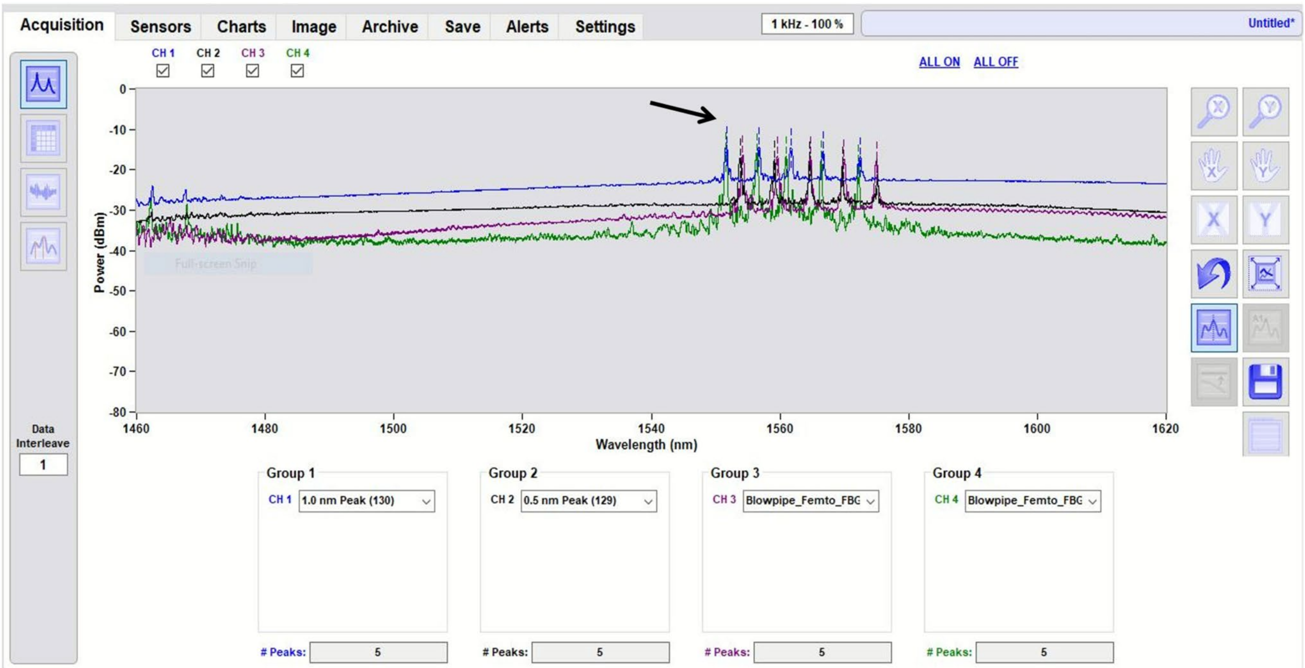

Fig. 6 Peaks detected in four FBG sensor arrays for temperature measurement

Fig. 7 Comparison of numerical simulation and experimental data acquired from FBG sensors

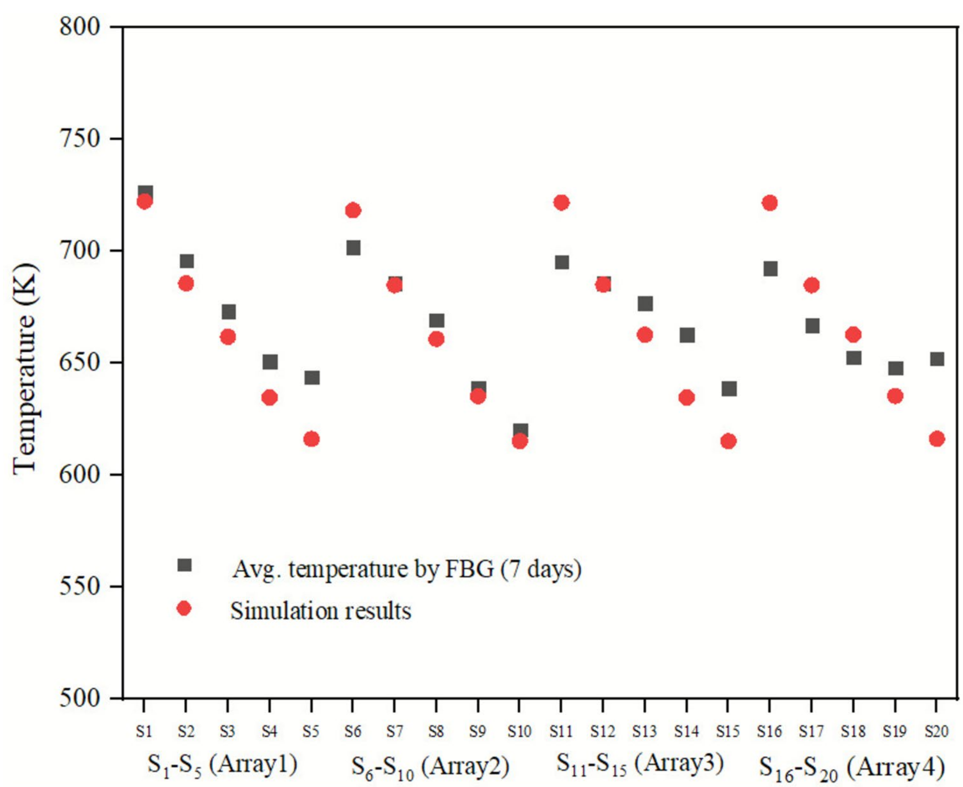

possibly due to the uneven grinding process on the surface during the embedding of the FBG sensors. The root-mean-square error (RMSE) value for the validation with simulation data was found to be 18.197 K. This shows a very close temperature difference in real-time temperature monitoring.

4 Conclusion

Effective temperature monitoring of the blowpipe in a blast furnace is crucial for preventing catastrophic damage caused by an eroded refractory lining. The numerical conjugate heat transfer model was applied to the ideal blowpipe case and potential anomaly scenarios of the blowpipe refractory liner to determine the temperature distribution on the surface of the blowpipe. This distribution facilitated the placement of the sensor on the blowpipe surface during experimentation. Furthermore, the numerical simulation of the blowpipe temperature profile for an ideal case, without any defects in the blowpipe structure, was validated experimentally using FBG-based temperature measurement. A similar trend was observed in the real-time temperature information gathered from the sensors over the 7-day average temperature measurement period. The RMSE value for the measurement, 18.197 K, is trivial in the high-temperature environment, which may have arisen due to uneven grinding depth and sensor embedment on the blowpipe surface. Further enhancement in detection performance can be achieved through the development of specialized blowpipes that incorporate provisions for embedding a uniform sensor array across the entire surface.

5 Future Scope

Using the present approach, anomaly estimation can be developed at different locations by performing multiple synthetic combinations of refractory lining erosion. The generated data can then be used to train machine learning models to predict anomalies caused by refractory liner erosion. The present work will serve as a precursor to the development of an ML system. The simulation data and real-time temperature data will be used to train the ML model for the prediction of hotspots in the blowpipe. This ML system will be helpful for alerting the industry personnel to any precautionary actions. Thus, by combining state-of-the-art embedded temperature sensor technology, advanced simulation models, and machine learning algorithms, this method may ensure maximum safety and efficiency in blast furnace operations, preventing catastrophic failures.

Acknowledgements The authors express their gratitude to the Directors of CSIR-NML, CSIR-CGCRI, and Tata Steel Limited for providing the necessary infrastructure to conduct the investigation and for permitting the publication of this work. The authors would like to acknowledge funding by M/s Tata Steel, Jamshedpur, and the Central Scientific and Industrial Research (CSIR), New Delhi.

Author Contributions All authors contributed to the study. The study was conceptualized by SPS, SB (CGCRI), and SB (Tata Steel). CFD numerical analysis was performed by YU. Data collection, sensor location optimization, and data analysis were performed by YU, ST, CD, AK, AG, and SPS. FBG sensors were fabricated and packaged by PD and SB(CGCRI). Industrial implementation was carried out by CD, AK, ST, TKD, PD, RSS, and SB (Tata Steel). All authors read and approved the final manuscript.

Funding Tata Steel,CLP0216,Sarmishtha Palit Sagar,Council of Scientific and Industrial Research,India,HCP0042—WP 1.1,Sarmishtha Palit Sagar

Declarations

Conflict of interest Authors have no financial or non-financial interests that are directly or indirectly related to the work submitted for publication.

References

1. Cakir M, Guvenc M A, and Mistikoglu S, *Comput. Ind. Eng.* **151** (2021) 106948. https://doi.org/10.1016/j.cie.2020.106948
2. Uguz S, and Ipek O, *J. Intell. Manuf.* **33** (2022) 1393. https://doi.org/10.1007/s10845-020-01729-0
3. Silvestri L, *Procedia Comput. Sci.* **180** (2021) 381. https://doi.org/10.1016/j.procs.2021.01.359
4. Richard D, Jang J, Çıtmacı B, Luo J, Canuso V, Korambath P, Morales-Leslie O, Davis J F, Malkani H, Christofides P D, and Morales-Guio C G, *Iscience* **26** (2023) 1. https://doi.org/10.1016/j.isci.2023.106966
5. Chen J, Young B, and Uy B, *J. Struct. Eng.* **132** (2006) 1948. https://doi.org/10.1061/(asce)0733-9445(2006)132:12(1948)
6. Falak P, Ebrahimzadeh I, and Jamneshan M, *J. Fail. Anal. Prev.* **19** (2019) 1691. https://doi.org/10.1007/s11668-019-00767-y
7. Sinha P, Mukhopadhyay G, and Bhattacharyya S, *J. Fail. Anal. Prev.* **13** (2013) 257. https://doi.org/10.1007/s11668-013-9666-5
8. Deshmukh S, and Dhamangaonkar P, *Mater. Today Proc.* **72** (2023) 768. https://doi.org/10.1016/j.matpr.2022.09.014
9. Lee J, Walla N, Silaen A K, Goodloe D D, and Zhou C Q, *Iron Steel Technol.* **16** (2019) 54.
10. Nielson S, Okosun T, Damstedt B, Jampani M, and Zhou C Q, *Processes.* **9** (2021) 1447. https://doi.org/10.3390/pr9081447
11. Usha Y, Tewary S, Ghosh A, Dutta C, Metya A K, and Palit Sagar S, Numerical Simulation to Predict Critical Hotspot Temperature in Blast Furnace Blowpipe to Avoid Industrial Hazard BT - Advances in Non-Destructive Evaluation. in *Conference and Exhibition on Non Destructive Evaluation*, Singapore, Springer Nature Singapore (2022), pp 1–7.
12. Mishra B, Padhee P R, Singh R K, Sahoo D R, and Mishra S, *Trans. Indian Inst. Met.* **73** (2020) 2191. https://doi.org/10.1007/s12666-020-02022-7
13. Sahota J K, Gupta N, and Dhawan D, *Opt. Eng.* **59** (2020) 1. https://doi.org/10.1117/1.oe.59.6.060901
14. Ansys Fluent 18 (2018) ANSYS Fluent Tutorial Guide 18. ANSYS Fluent Tutor. Guid. 18, vol. 15317, April, pp. 724–746

15. Werneck MM, Allil RC, Ribeiro BA, De Nazaré FV (2013) A guide to fiber Bragg grating sensors. Current trends in short-and long-period fiber gratings. 1-24
16. Biswas P, et al., *Sensors Actuators, A Phys.* **157** (2010) 77. https://doi.org/10.1016/j.sna.2009.10.020
17. Morey W W, Meltz G, and Glenn W H, *Fiber optic and laser sensors VII* **1169** (1990) 98.
18. Broadway C, Min R, Leal-Junior A G, Marques C, and Caucheteur C, *J. Light. Technol.* **37** (2019) 2605. https://doi.org/10.1109/JLT.2018.2885957
19. Leal-Junior A G, and Marques C, *IEEE Sens. J.* **21** (2021) 12719. https://doi.org/10.1109/JSEN.2020.3040987
20. Diaz C A R, Leal-Junior A G, Avellar L M, Antunes P F C, Pontes M J, Marques C A, Frizera A, and Ribeiro M R N, *Sensors.* **19** (2019) 2962.
21. Díaz C A R, et al., *Sensors (Switzerland)* **17** (2017) 1. https://doi.org/10.3390/s17102414